Shape from Water: Bispectral Light Absorption for Depth Recovery

Yuta Asano[1], Yinqiang Zheng[2(✉)], Ko Nishino[3], and Imari Sato[1,2]

[1] Department of Information Processing,
Tokyo Institute of Technology, Meguro, Japan
asano.y.ac@m.titech.ac.jp
[2] Digital Content and Media Sciences Division,
National Institute of Informatics, Tokyo, Japan
{yqzheng,imarik}@nii.ac.jp
[3] Department of Computer Science, Drexel University, Philadelphia, USA
kon@drexel.edu

Abstract. This paper introduces a novel depth recovery method based on light absorption in water. Water absorbs light at almost all wavelengths whose absorption coefficient is related to the wavelength. Based on the Beer-Lambert model, we introduce a bispectral depth recovery method that leverages the light absorption difference between two near-infrared wavelengths captured with a distant point source and orthographic cameras. Through extensive analysis, we show that accurate depth can be recovered irrespective of the surface texture and reflectance, and introduce algorithms to correct for nonidealities of a practical implementation, including tilted light source and camera placement and nonideal bandpass filters. We construct a coaxial bispectral depth imaging system using low-cost off-the-shelf hardware and demonstrate its use for recovering the shapes of complex and dynamic objects in water. Experimental results validate the theory and practical implementation of this novel depth recovery paradigm, which we refer to as shape from water.

Keywords: Depth recovery · Light absorption · Multispectral imaging

1 Introduction

Three-dimensional geometry recovery has been one of the central focuses of research in computer vision from its inception due to the fundamental role 3D geometry may play in almost all applications. These research efforts have culminated in the establishment of a handful of distinct principles for modern shape recovery methods, including triangulation, time of flight, and shape-from-X where X can be shading, texture, focus, and other surface or image formation properties. The fundamental but often neglected assumption of these different approaches is that the light, either actively or passively shed on the object surface including environmental illumination, can be measured unaltered between the surface and the camera. Although there are some works that study shape

B. Leibe et al. (Eds.): ECCV 2016, Part VI, LNCS 9910, pp. 635–649, 2016.
DOI: 10.1007/978-3-319-46466-4_38

recovery of objects in non-air medium where this assumption does not hold (e.g., participating medium like dilute milk), their focus is on undoing the adversarial optical perturbations such as scattering to apply the same recovery principals that were designed for objects in clear air. In other words, the medium is treated as an unwanted nuisance that violates the assumed geometry recovery principle.

Can we instead exploit whatever may happen to the light as it travels from the surface to the camera for shape recovery? If we can, what advantages would it give us? In the past, scattering has been modeled to restore clear day scene appearance from images taken in bad weather conditions (e.g., fog), in whose process the scene depth can also be recovered. This, however, is limited to accidental imaging in bad weather conditions, and cannot be used as a general shape recovery method. In this paper, we focus on light absorption in the infrared spectrum as a light propagation characteristic that encodes depth. When light travels through a homogeneous isotropic medium, it usually gets absorbed at some wavelengths. The light absorption is dictated by the Beer-Lambert law, which denotes the absorption at a certain wavelength to be proportional to the length of the light travel path and to the absorption coefficient of the medium [12]. This suggests that we may recover the distance of a surface point to the camera by measuring the amount of light absorption that takes place between the surface and the camera. In other words, we may recover depth of an object by measuring the light path distance (i.e., optical depth) from the camera of the medium in between.

In this paper, we focus on water as the medium for a few important reasons. In addition to the fact that water is a familiar liquid that we can easily find in our daily lives, geometry recovery in water in itself finds applications in many areas of science such as oceanography, geography, and biology, as well as engineering including underwater surveillance and navigation. Furthermore, multi-spectral light propagation in water is mostly dominated by absorption and scattering plays little effect as long as the water is sufficiently clear, which would otherwise compound the optical length computation. Few past methods have directly applied the depth recovery principals in air to underwater scenarios, and have found light absorption to adversely affect the results [2]. We instead take advantage of light absorption in water and establish shape from water as a novel shape recovery approach.

We propose a novel shape recovery method based on monochromatic images captured at two different infrared wavelengths, which we refer to as the bispectral principle of depth recovery. The key idea is to exploit the difference in the amount of light absorption that takes place at two distinct wavelength and cancel out light interaction effects, including those due to surface texture and reflectance, other than that proportional to the optical length to the object surface. Figure 1 shows an example of recovering a textureless, specular object which would be a challenging object for conventional depth recovery methods.

We thoroughly analyze the theory including its limitations as well as practical accuracy of the proposed method. In particular, we examine the effect of reflectance spectrum difference of the object at the two working wavelengths,

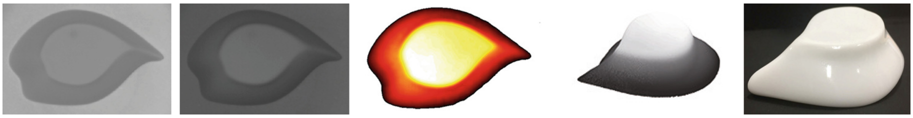

(a) 905nm (b) 950nm (c) Depth coded (d) 3D shape (e) RGB

Fig. 1. Shape from water based on bispectral light absorption. (a) and (b) show the scene at 905 nm and 950 nm, after normalizing the illumination and camera and filter sensitivity functions. The intensity difference between (a) and (b) is due to the difference of water absorption at these two wavelengths which we exploit to recover the depth. The color coded depth is shown in (c), and the recovered 3D shape is given in (d). (e) shows the target object for this example: a textureless ceramic object with strong specularity.

and develop a criterion to properly choose the two wavelengths so as to maximize the difference of the absorption coefficient and minimize the dependence on material spectral reflectance. We also propose correction algorithms to handle those factors arising from practical implementation limitations of our bispectral principle, including the effects of tilting the light source and/or the camera with respect to the water surface and the effects of nonideal spectral bandpass filters.

We build a co-axial bispectral imaging system using low-cost off-the-shelf hardware as a prototype implementation for single exposure, real-time shape from water. The system consists of two monochromatic cameras equipped with near-infrared bandpass filters, aligned on the same optical axis with a half beam splitter. We envision use of shape from water with a bispectral imaging system immersed in water, but for practical reasons, all experiments are done with a water tank and the co-axial system placed outside of it. Experimental results validate the theory of our bispectral light absorption depth imaging principle, and demonstrate its advantages over conventional approaches.

Our major contributions can be summarized as follows.

- We introduce light absorption as a means to depth sensing in computer vision.
- We derive the bispectral light absorption principle for depth recovery and apply it to water leading to shape from water.
- We thoroughly analyze the theory and practical implications of shape from water.
- We construct a low-cost co-axial bispectral imaging system and demonstrate its use for dense shape recovery of complex and dynamic objects in water.

Taken together, for the first time, we introduce a new shape recovery method based on light absorption in water and its working prototype that achieves shape recovery of complex, dynamic objects.

2 Related Works

Most popular shape recovery methods can be categorized based on the underlying shape or depth probing principles: triangulation, time of flight, and shape-from-X where shading is most prominent for X but may include other surface and image formation properties like texture and focus. The literature for each is vast and readers may find suitable survey articles elsewhere.

Triangulation is the fundamental geometric relation exploited in binocular or multiview stereo, and structure from motion [5]. If correspondence could be reliably established, sparse or even dense 3D shape can be recovered. The fundamental limitation of triangulation is that sufficient (unique) texture must be found on the surface to establish those correspondences. Structured active light can mitigate this limitation [1] by essentially putting texture on the surface, by actively projecting visible or infrared light patterns.

Time of flight, the travel time of a light pulse to hit a surface and come back to the source, directly encodes the distance of the surface from the source [4]. Coherent light (e.g., laser) can be used for long-distance depth sensing, while infra-red light has been recently used for short-distance measurements (e.g., Kinect 2). Accurate measurement of time of flight is challenging due to the very high speed of light and can limit the resolution of the depth image.

Shape-from-X refers to shape recovery methods that exploit specific surface or image formation properties. Among the many radiometric cues, shading so far has been one of the most popular. Shape-from-shading [17] and photometric stereo [16] model the surface brightness change to infer its gradients (i.e., surface normals) from which the shape can be recovered. In contrast to triangulation-based methods, texture as well as complex reflectance (i.e., non-Lambertian surfaces) become nuisances that hinder the applicability of these methods.

In this paper, we introduce a novel bispectral depth imaging principle based on light absorption. It clearly differs from triangulation and other shape-from-X, especially shading, methods in that it neither requires feature correspondence nor known or simplistic surface reflectance. Unlike time-of-flight methods, it recovers depth by measuring pixel intensity difference, in contrast to light travel time, which obviates the need of often expensive hardware for accurate temporal measurement.

Shape recovery in non-air medium has been studied in the past. Narasimhan et al. [10] apply light stripe range scanning and photometric stereo to objects in participating media. They model sub-surface scattering and account for it to recover object geometry in murky water (e.g., dilute milk). Light scattering has also been studied in computer vision for other participating media such as fog [3,6,7,9,11,13,14] in which depth can be recovered in the process of removing the light propagation effects on the appearance (i.e., defogging). Our depth recovery principle is similar to such approaches in that it actively exploits the light propagation characteristics in the medium to decode the optical length and thus depth. Our focus is, however, light absorption, not scattering.

A number of underwater depth recovery methods have been introduced in the past. For example, Tomohiko et al. [15] used multiview stereo to reconstruct underwater objects, and their focus was on accounting for the refractive effect of water and the shape of the interfacing layer (glass wall of the container here). Murez et al. [8] applied photometric stereo to underwater objects, and tried to handle the scattering problem due to water turbidity. Dancu et al. [2] evaluated the performance of various time-of-flight sensors to reconstruct underwater objects, and found that these sensors do not work for slightly deep water, because of severe infrared light absorption of water.

3 Light Absorption in Water

Let us first review the basics of light absorption in water. When light travels in water, it gets absorbed at some wavelengths. The absorption curve in Fig. 2(a) shows how light will be attenuated as it travels through water (with 6 mm depth here), in the wavelength range from 400 nm to 1400 nm. From this curve, we can observe that water rarely absorbs visible light, which explains why water appears transparent to human eyes. In contrast, it clearly absorbs infrared light from 900 nm to 1400 nm.

As illustrated in Fig. 2(b), at a given wavelength λ, the Beer-Lambert law [12] accurately expresses light absorption as the relation between incident light intensity I_0 and outgoing attenuated intensity I

$$I = I_0 e^{-\alpha(\lambda) l}, \tag{1}$$

in which l represents the light path length in millimeter (mm), $\alpha(\lambda)$ denotes the wavelength dependent absorption coefficient in mm^{-1}, and $e^{-\alpha(\lambda) l}$ is the natural exponential of $-\alpha(\lambda) l$.

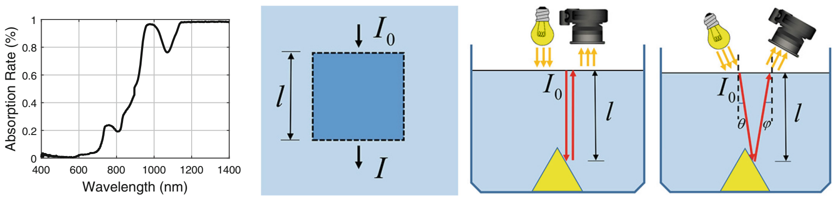

(a) Water absorbance (b) Beer-Lambert (c) Coaligned (d) Tilted

Fig. 2. (a) shows the water absorption curve in the range from 400 nm to 1600 nm. (b) shows the setup of the Beer-Lambert law. (c) and (d) illustrate our bispectral depth imaging in the coaligned and tilted configuration, respectively.

4 Bispectral Light Absorption for Depth Recovery

We will exploit the wavelength dependence of light absorption for depth recovery of objects immersed in water. We assume that the camera is orthographic and the incident light rays to the object surface are parallel coming from an infinitely distant point source. Yet, we do not make assumptions on the surface reflectance such as Lambertian or diffuse plus specular, except that the geometric and spectral characteristics of the reflectance are separable. This is a very mild assumption that assumes that the reflectance function $f(\omega, \lambda) = r(\omega)s(\lambda)$ can be factorized into its geometric properties (e.g., incident and exitant light angles), $r(\omega)$, and spectral characteristics (i.e., color), $s(\lambda)$, which applies to most real-world surfaces. The only exceptions are when the surface geometry intricacies are comparable to light wavelength in scale (e.g., CD-ROM). Most importantly, we envision an imaging system fully immersed in the water, in which the consideration of water surface is unnecessary, but for all practical necessity, we place the camera and light source outside the water. As we assume directional light and orthographic cameras and use sufficiently close wavelengths, we may safely ignore the effects of light refraction at the water surface.

4.1 Bispectral Depth Imaging

As illustrated in Fig. 2(c), we first consider an ideally coaligned light-camera configuration, in which both the optical axis of the camera and the directional light are perpendicular to the planar water surface. Monochromatic light of wavelength λ_1 and intensity I_0 reaches an opaque scene point with water depth l. After being reflected back from the scene point, the intensity of the light received by the camera is

$$I(\lambda_1) = r(\omega)s(\lambda_1)I_0 e^{-2\alpha(\lambda_1)l}, \tag{2}$$

in which $2l$ denotes light travel distance which is twice as long as the water depth l.

The geometric and spectral characteristics of surface reflectance, $r(\omega)$ and $s(\lambda_1)$, respectively, are related to the underlying surface material composition which is, of course, unknown. To cancel out this unknown, we use a second monochromatic observation at wavelength λ_2 with a corresponding light source of the same intensity I_0. The radiance received by the camera for the second light beam will be

$$I(\lambda_2) = r(\omega)s(\lambda_2)I_0 e^{-2\alpha(\lambda_2)l}. \tag{3}$$

By dividing Eq. (2) by Eq. (3), the depth l can be estimated as

$$l = \frac{1}{2(\alpha(\lambda_2) - \alpha(\lambda_1))} \ln \left(\frac{I(\lambda_1)}{I(\lambda_2)} \frac{s(\lambda_2)}{s(\lambda_1)} \right). \tag{4}$$

It is interesting to note that the geometric factor of the reflectance function $r(\omega)$ has been eliminated, no matter how complex it is. Provided that we can choose two wavelengthes such that the reflectance spectrum values at these two wavelengthes are almost identical, i.e., $s(\lambda_1) \simeq s(\lambda_2)$, the approximate depth can be recovered,

$$l \simeq \frac{1}{2\left(\alpha(\lambda_2) - \alpha(\lambda_1)\right)} \ln \frac{I(\lambda_1)}{I(\lambda_2)}. \tag{5}$$

Equation (5) stays at the core of our bispectral depth recovery principle, which allows us to estimate depth simply by measuring the pixel intensity difference at two properly chosen wavelengths, without knowing any information of the arbitrarily general reflectance function of the scene point material.

4.2 Depth Accuracy and Surface Reflectance

Let us first analyze the relative depth error $\triangle l$ with respect to the relative difference $\triangle s$ between $s(\lambda_1)$ and $s(\lambda_2)$, which is defined as $\triangle s = s(\lambda_1)/s(\lambda_2)$-1.

According to Eqs. (4) and (5), the relative depth error $\triangle l$ can be calculated by

$$\triangle l = \frac{\ln\left(\frac{I(\lambda_1)}{I(\lambda_2)}\frac{s(\lambda_2)}{s(\lambda_1)}\right) - \ln\frac{I(\lambda_1)}{I(\lambda_2)}}{\ln\left(\frac{I(\lambda_1)}{I(\lambda_2)}\frac{s(\lambda_2)}{s(\lambda_1)}\right)} = \frac{\ln(1+\triangle s)}{\ln(1+\triangle s) - \ln\frac{I(\lambda_1)}{I(\lambda_2)}}. \tag{6}$$

Figure 3(a) shows relative depth error plotted against relative reflectance difference for varying intensity ratios $I(\lambda_1)/I(\lambda_2)$. From these curves, we can observe that the estimated depth becomes less sensitive to the reflectance spectrum difference, as the intensity ratio steps away from one (i.e., the difference between the two wavelengths becomes larger). This suggests a criterion for choosing the two wavelengths for bispectral depth recovery. Specifically, we should choose two wavelengths whose water absorption coefficients' difference is maximized, while the corresponding reflectance spectrum difference is minimized.

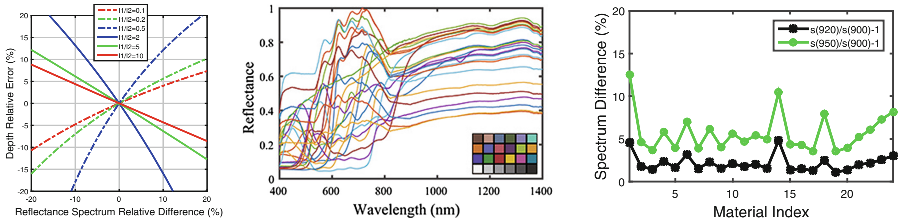

(a) Depth error (b) Spectra of 24 patches (c) Spectrum difference

Fig. 3. (a) shows relative depth error with respect to the reflectance spectrum difference, under varying intensity ratios. (b) shows the spectra of the 24 patches on the color checker in the range from 400 nm to 1400 nm. The reflectance spectrum difference for spectral pairs of 900 nm and 920 nm, as well as 900 nm and 950 nm for each patch spectrum is shown in (c). (Color figure online)

As shown in Fig. 2(a), the amount of light absorption in water changes quickly in the range between 900 nm and 1000 nm. Surprisingly, we empirically find that the reflectance spectra of a great variety of materials tend to be flat (i.e., spectrally white) in this range.

We start our investigation by examining the spectra of the standard color checker board, as shown in Fig. 3(b), from which we can clearly observe that the spectral variance for all patches drastically reduces in the range longer than 900 nm. As shown in Fig. 3(c), although there are a few patches with larger difference, the average relative spectrum difference for 900 nm and 950 nm is 5.7 %, which will further reduce to 2.1 % for the spectral pair of 900 nm and 920 nm.

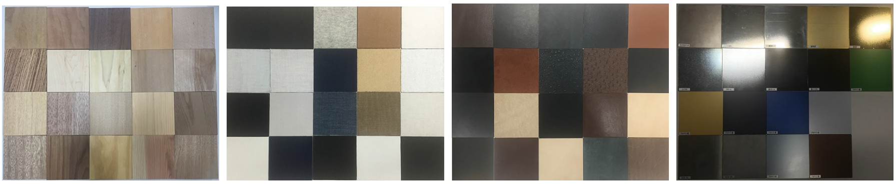

(a) Four classes of materials (From left to right: wood, cloth, leather and metal)

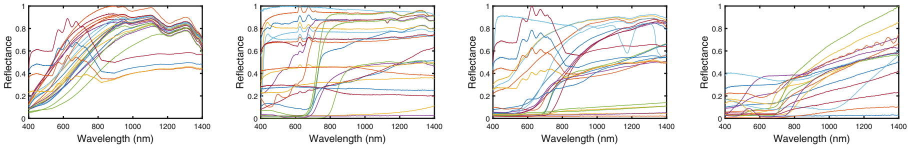

(b) Reflectance spectra of the materials

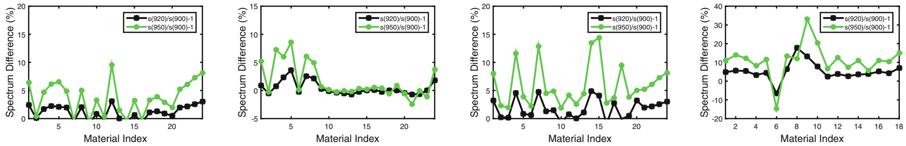

(c) Relative reflectance spectrum difference

Fig. 4. A reflectance spectra database in the Vis-NIR range from 400 nm to 1400 nm. We empirically find that the spectral reflectance difference for two close near-infrared wavelengths is usually negligible.

We have also collected several other classes of common materials, including wood, cloth, leather and metal, as shown in Fig. 4(a). There are 24 different materials in each class, except metal which has only 18. We measure their reflectance spectra and evaluate the reflectance spectrum difference for wavelength pairs of 900 nm and 920 nm, as well as 900 nm and 950 nm. The average relative spectrum difference of these four classes for the bispectral pair 900 nm and 950 nm is 3.8 %, 2.1 %, 6.0 % and 11.1 %, respectively. For the bispectral pair 900 nm and 920 nm, the corresponding average difference reduces to 1.4 %, 1.1 %, 1.9 % and 5.0 %. Although the scale of our database is limited, the evaluation result suggests that the reflectance spectrum difference is usually very small for two close near-infrared wavelengths.

5 Practical Shape from Water

We derive algorithms for shape from water with practical setups based on the bispectral depth recovery principle. In particular, we propose two algorithms that correct distorted depth estimates resulting from nonidealities in the imaging setup.

5.1 Non-collinear/Perpendicular Light-Camera Configuration

Until now, we have considered the collinear light-camera configuration, in which both the optical axis of the orthographic camera and the directional light are perpendicular to the water level. In practice, the light rays and/or the camera might be slightly tilted from the water surface, due to practical requirements of the system setup. Here, we will show that, if the depth of a single point is given, the depth distortion can be corrected.

As illustrated in Fig. 2(d), the tilt angles in water for the illuminant and the camera are denoted by θ and ψ, respectively. Note that, the refractive ratio of water is almost constant in the near-infrared range. Therefore, we can assume that these two angles do not change at the two working wavelengths. The light path length is stretched to $l(\frac{1}{\cos\theta} + \frac{1}{\cos\psi})$, rather than $2l$. Similar to Eq. (5), now the depth can be calculated by

$$l(\frac{1}{\cos\theta} + \frac{1}{\cos\psi}) \simeq \frac{1}{\alpha(\lambda_2) - \alpha(\lambda_1)} \ln \frac{I(\lambda_1)}{I(\lambda_2)}, \tag{7}$$

from which we can observe that, if the depth of a single point is provided, the distortion factor $(\frac{1}{\cos\theta} + \frac{1}{\cos\psi})$ can be easily estimated.

5.2 Nonideal Narrow-Band Filters

When implementing a bispectral imaging system for shape from water, it is preferable to use a wide-band illuminant and two narrow-band filters in front of the camera. Until now, we have implicitly assumed that the response function of the filters is a delta function (i.e., perfect narrow-band), which is hard to achieve in practice.

Let us denote the spectral response functions of two nonideal narrow-band filters each centered at λ_1 and λ_2 with $\beta_1(\lambda)$ and $\beta_2(\lambda)$, respectively. If the band-pass filters are sufficiently narrow, we can assume that the reflectance spectrum of the scene point is flat between the two wavelengths. The imaging equation Eq. (2) becomes

$$I(\lambda_1) = r(\omega)s(\lambda_1)I_0 \int_0^\infty \beta_1(\lambda)e^{-2\alpha(\lambda)l} d\lambda. \tag{8}$$

A similar equation can be established for Eq. (3). The depth l can be corrected by solving the following equation

$$I(\lambda_1) \int_0^\infty \beta_2(\lambda)e^{-2\alpha(\lambda)l} d\lambda = I(\lambda_2) \int_0^\infty \beta_1(\lambda)e^{-2\alpha(\lambda)l} d\lambda, \tag{9}$$

using standard one-dimensional zero-finding techniques. Note that we do not explicitly consider the illumination spectrum and the camera spectral sensitivity function, since they can be merged into the spectral response function of the filters.

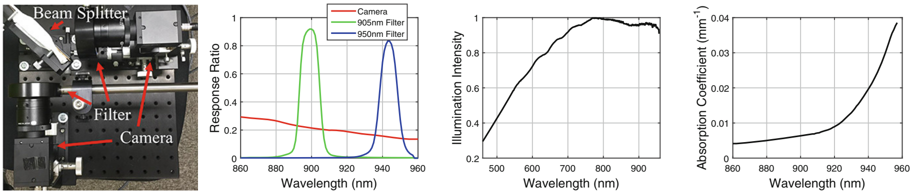

(a) System (b) Spectral response (c) Illumination (d) Absorp. coeff.

Fig. 5. (a) shows our co-axial bispectral imaging system, and (b) the spectral response functions of the camera and the two filters. (c) is the spectrum of the incandescent illuminant. (d) is the calibrated water absorption coefficient.

6 Co-Axial Bispectral Imaging System and Experiment Results

We built a co-axial bispectral imaging system for shape from water. The system uses co-axial cameras to simultaneously capture the scene in two wavelengths, recording bispectral image pairs at video-rate. From the image sequence, we may recover the geometry of complex and dynamic objects immersed in water.

6.1 System Configuration and Calibration

As shown in Fig. 5(a), the co-axial bispectral imaging system consists of a beam splitter and two grayscale cameras (POINTGREY GS3-U3-41C6NIR), which can sense NIR light albeit with limited spectral sensitivity. We use two narrow band-pass filters centered at 905 nm and 950 nm, whose spectral response curves are shown in Fig. 5(b). For the illumination, we use an incandescent lamp with sufficient irradiance in the NIR range, as shown in Fig. 5(c). We synchronize the two cameras, and carefully adjust the position of the beam splitter to capture spatially-aligned bispectral image pairs of the same scene.

The water absorption coefficient needs to be known for shape from water, which can be estimated easily beforehand. We use a spectrophotometer and a standard white target for calibration. By immersing the white target into water at a known depth, we can calculate the water absorption coefficient from the Beer-Lambert law. Figure 5(d) illustrates the calibrated absorption coefficient for different wavelengths.

6.2 Depth and Shape Accuracy

We use planar plates with different materials for depth accuracy evaluation. We put the plates in water and measure the water depth by a ruler for ground truth. We vary the water depth from 10 mm to 40 mm. At each depth, we capture two images with our co-axial bispectral system and estimate the depth using Eq. (5). To evaluate the effectiveness of our algorithms in Sect. 5, we also correct the depth further by using Eqs. (7) and (9).

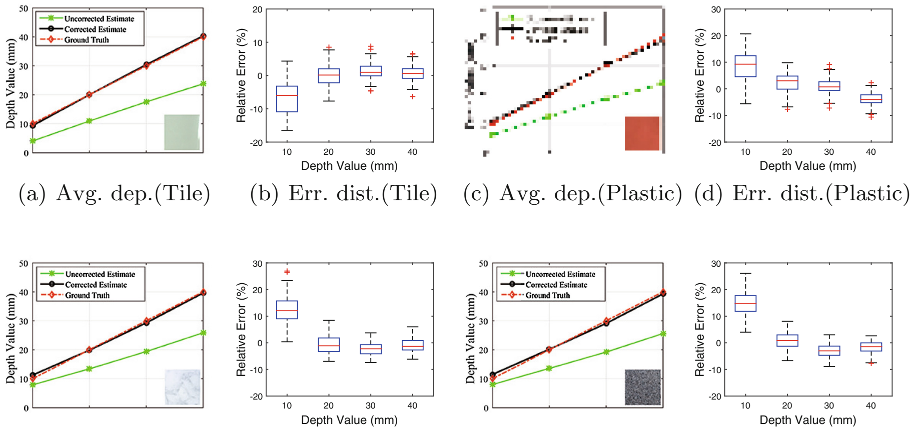

(a) Avg. dep.(Tile) (b) Err. dist.(Tile) (c) Avg. dep.(Plastic) (d) Err. dist.(Plastic)

(e) Avg. dep.(WM) (f) Err. dist.(WM) (g) Avg. dep.(BM) (h) Err. dist.(BM)

Fig. 6. Depth estimation error for four planar plates, including cyan tile, red plastic board, white marble (WM) and black marble (BM). (Color figure online)

As shown in Fig. 6, we use four plates for experiments, including a piece of cyan tile, a red plastic board, a piece of white and black marble. On each plate, we randomly choose 121 points (pixels), and calculate the average depth for these points. To evaluate the spatial consistency of the depth estimate at each depth, we draw the distribution of the relative error of the corrected depth for these 121 points in Fig. 6(b,d,f,h). The values between the 25 and 75 percentiles are shown as a box with a horizontal line at the mean value. The red crosses indicate data beyond 1.5 times the inter-percentile range.

From Fig. 6, we can observe that the correction algorithms play a critical role in improving the estimation accuracy. With correction, the average depth estimates are very close to the ground truth, usually within a relative error of 3 %. However, the average depth error is clearly higher at 10 mm depth. The main reason for this is that we measure the ground truth with a ruler, which introduced errors at this distance. As for the spatial consistency of the depth estimates, we can observe that the corrected depth at the measured 121 points is sufficiently consistent with each other, even when the plate assumes spatially varying textures (e.g., the marble plate).

6.3 Complex Static and Dynamic Objects

We apply shape from water to objects with complex reflectance and dynamically moving objects whose shape deforms. Since the ground truth shape is difficult to capture for these objects, we qualitatively evaluate the recovered geometry.

Figure 7 shows the recovery results of several opaque objects with varying color, texture, and reflectance properties. We can observe that our system and method work well for textureless objects with strong specularities. The surface reflectance and geometry of the seashell and rock in the first and second row

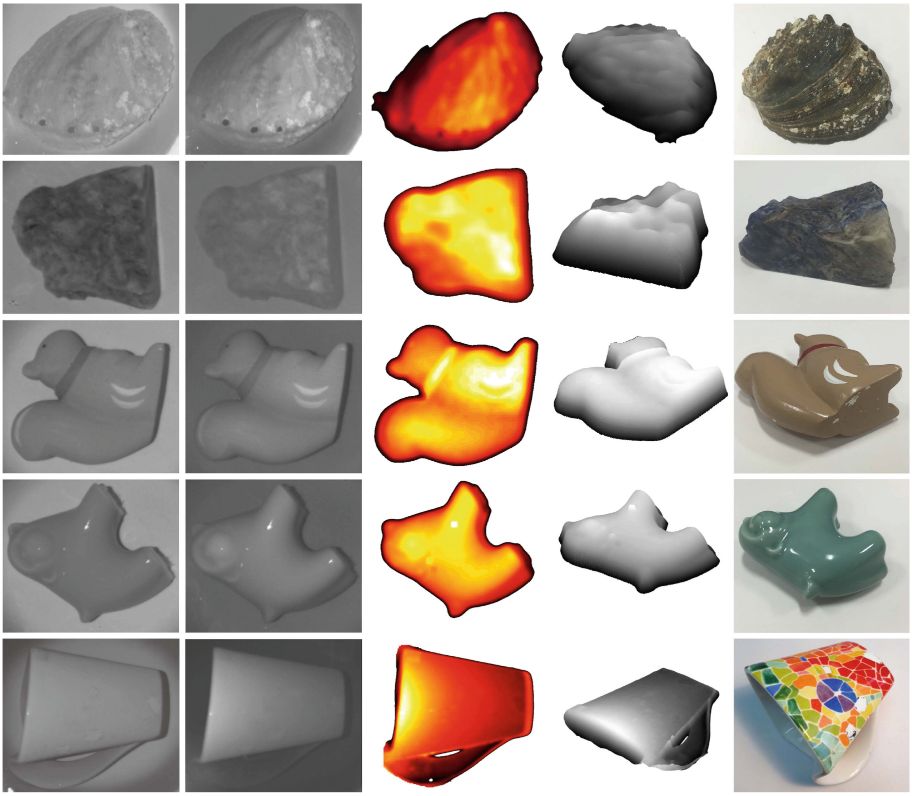

Fig. 7. Shape recovery of objects with complex geometry, texture, and reflection properties. For each row, from left to right, the input images at 905 nm and 950 nm, the depth coded 3D shape, the virtually shaded shape and the RGB appearance of the object are shown. (Color figure online)

of Fig. 7 are particularly complicated, and would pose significant challenges to other shape recovery methods. The results clearly show that shape from water, as the theory shows, is insensitive to such intricacies. This property is verified again by the compelling results for the colorful cups in the last row of Fig. 7. We also note that artifacts due to specularities sometimes occur (fourth row), which is attributed to camera saturation, rather than the method itself.

Figure 8 shows the recovery results of some even more challenging objects with translucence. The recovered shape looks compelling, when compared it with its corresponding RGB appearance.

Our co-axial shape from water system is suited to capture dynamic scenes. As shown in Fig. 9, we demonstrate this by recovering the geometry of a moving hand in water.

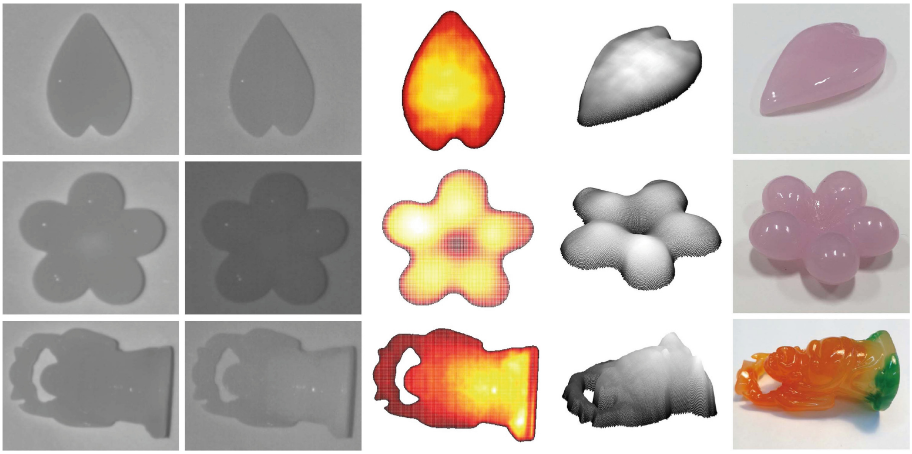

Fig. 8. Shape recovery of translucent objects.

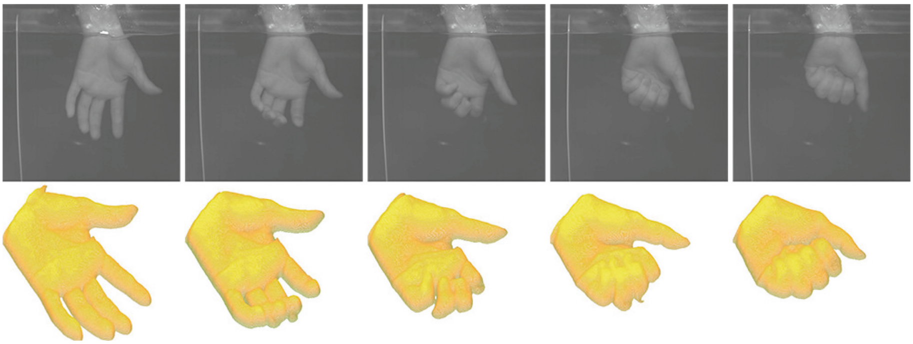

Fig. 9. Action capturing of a moving hand in water.

Fig. 10. Recovery of a transparent glass object. From left to right are the RGB image (a side view of the glass at 905 nm in the corner shows that the glass is also transparent under NIR light), 3D shape from a laser scanner, RGB image of the same object with painting, 3D shape from a laser scanner with painting, and 3D shape from our method without painting. (Color figure online)

7 Discussions

Bispectral depth recovery in its current form is not able to directly handle environment illumination. In practice, it can be eliminated by taking another pair of images under the environment illumination only, and subtracting them away from the input image pair under mixed illumination.

Surface reflection occurs at the water surface, which will lead to erroneous depth for a shape-from-water imaging system situated outside water surface. We have found that this problem can be alleviated by simply taking one image without any object but only a black, infrared light absorbing, material in the water that captures the water surface reflection alone and subtracting it from the observation pairs.

Similar to most existing depth imaging principles and techniques, our principle is vulnerable to interreflection, often not negligible for concave surfaces, and tends to smooth out shape details, as can be observed for the statue in the third row of Fig. 8.

Shape reconstruction of transparent objects is challenging for contact-free depth imaging. For shape from water, if the material happens not to absorb near-infrared light, which is actually the case for many kinds of glasses, and the light does not travel to the water behind the object (e.g., the bottom side of the object is opaque), we can safely recover the surface geometry, as shown in Fig. 10. Note that the 3D laser scanner can not correctly capture the shape of the glass surface, unless it is uniformly painted.

The analysis in Sect. 4.2 implies that choosing two wavelengths with drastically different absorption coefficients would benefit depth recovery accuracy. That's one major reason why we have used two images at 905 nm and 950 nm. However, due to strong absorption, the image at 950 nm will be very dark, when the object is slightly far away from the camera. One idea to resolve the resulting poor SNR issue is to choose three shorter wavelengths with less absorption, and assume instead that the reflectance spectrum values at these three wavelengths are collinear. The details will be explored in near future.

8 Conclusions

In this paper, we introduced shape from water, a novel depth recovery method based on light absorption in water. Shape from water builds on the newly derived bispectral depth sensing principle based on the idea of leveraging the light absorption difference between two near-infrared wavelengths to estimate depth regardless of the surface reflectance. We constructed a co-axial bispectral depth imaging system using low-cost off-the-shelf hardware to capture bispectral image pairs for shape from water at video-rate. Experimental results show that shape from water can recover accurate geometry of objects with complex reflectance and dynamically deforming shapes.

Acknowledgments. This research was supported in part by the Ministry of Education, Science, Sports and Culture Grant-in-Aid for Scientific Research on Innovative Areas.

References

1. Batlle, J., Mouaddib, E., Salvi, J.: Recent progress in coded structured light as a technique to solve the correspondence problem: a survey. Pattern Recogn. **31**(7), 963–982 (1998)
2. Dancu, A., Fourgeaud, M., Franjcic, Z., Avetisyan, R.: Underwater reconstruction using depth sensors. In: SIGGRAPH Asia Technical, Briefs, pp. 1–4 (2014)
3. Fattal, R.: Single image dehazing. Proc. ACM SIGGRAPH **27**, 1–9 (2008)
4. Hansard, M., Lee, S., Choi, O., Horaud, R.: Time-of-Flight Cameras: Principles, Methods and Applications. Springer, Heidelberg (2012)
5. Hartley, R., Zisserman, A.: Multiple View Geometry in Computer Vision, 2nd edn. Cambridge University Press, Cambridge (2003)
6. He, K., Sun, J.X.T.: Single image haze removal using dark channel prior. In: Proceedings of IEEE International Conference on Computer Vision and Pattern Recognition, vol. 1 (2009)
7. Kratz, L., Nishino, K.: Factorizing scene albedo and depth from a single foggy image. In: IEEE International Conference on Computer Vision, pp. 1701–1708 (2009)
8. Murez, Z., Treibitz, T., Ramamoorthi, R., Kriegman, D.: Photometric stereo in a scattering medium. In: ICCV, pp. 3415–3423 (2015)
9. Narasimhan, S.G., Nayar, S.K.: Vision and the atmosphere. Int. J. Comp. Vis. **48**(3), 233–254 (2002)
10. Narasimhan, S., Nayar, S., Sun, B., Koppal, S.: Structured light in scattering media. In: IEEE International Conference on Computer Vision (2005)
11. Nishino, K., Kratz, L., Lombardi, S.: Bayesian defogging. Int. J. Comput. Vis. **98**(2), 232–255 (2012)
12. Reinhard, E., Khan, E.A., Akyuz, A.O., Johnson, G.: Color Imaging: Fundamentals and Applications. CRC Press, Boca Raton (2008)
13. Schechner, Y.Y., Narasimhan, S.G., Nayar, S.K.: Instant dehazing of images using polarization. In: Proceedings of IEEE International Conference on Computer Vision and Pattern Recognition, vol. 1, pp. 325–332, June 2001
14. Tan, R.T.: Visibility in bad weather from a single image. In: Proceedings of IEEE International Conference on Computer Vision and Pattern Recognition, pp. 1–8, June 2008
15. Tomohiko, Y., Nobuhara, S., Matsuyama, T.: 3D shape from silhouettes in water for online novel-view synthesis. IPSJ Trans. Comput. Vis. Appl. **5**, 65–69 (2013)
16. Woodham, R.: Photometric method for determining surface orientation from multiple images. Opt. Eng. **19**(1), 191139 (1980)
17. Zhang, R., Tsai, P., Cryer, J., Shah, M.: Shape-from-shading: a survey. IEEE TPAMI **21**(8), 690–706 (1999)